The Incorporation of Ionization Effect in Organic Semiconductor Assists to Trigger Multilevel Resistive Memory Behaviors

Cheng Zhang,[a,b] Hua Li,*[a] Yanna Su,[a] Fei Yu,[b] Chao Li,[b] Qichun Zhang,*[b,c] Jianmei Lu*[a]

Experimental Procedures

Materials

All the chemicals such as 9H-carbazole, N-bromosuccinimide (NBS), 1-Butylbromide, 4-Pyridineboronic acid, Phosphorus oxychloride ($POCl_3$), Rhodanine-3-acetic acid (RDA), Tetrakis(triphenylphosphine)palladium ($Pd(P(Ph_3)_4$), Methyl trifluoromethanesulphonate (MeOTF) were purchased from the commercial source (TCI Co., Ltd) and used without further purification. All the solvents (e.g., dioxane, piperidine, etc.) were purchased from Sinopharm Chemical Reagent and Enox Co., Ltd.

Instrumentation

All ^{1}H-NMR spectra were measured by an Inova 400 MHz Fourier workstation. Ultraviolet-visible (UV-vis) absorption spectra and cyclic voltammetry were obtained using the UV-3600 spectrophotometer (Shimadzu) and the CorrTest Electrochemical Workstation analyzer at 298 K in respectively. Atomic force microscopy (AFM) measurements were carried out by an MFP-3DTM AFM instrument. X-ray diffraction (XRD) pattern was performed using an X'Pert-Pro MPD X-ray diffractometer. All electrical measurements of the devices were performed using Keithley 4200-SCS semiconductor parameter analyzer under ambient conditions without any encapsulation.

Device preparation

The indium-tin-oxide (ITO) glass substrate was precleaned with water, ethanol, and acetone in an ultrasonic bath for 20 min, in sequence. A 10 mg/ml solution of the compounds in o-dichlorobenzene or acetonitrile was filtered through membrane micro-filters with a pore size of 0.22 μm and then spin-coated onto the substrates with the speed of 800 rpm for 10 s and sequential 1300 rpm for 30 s. 100-nm-thickness top Al layer was thermally evaporated onto the film under 2×10^{-6} Torr through a customized shadow mask with a diameter of 1 mm under N_2 atmosphere.

Synthetic procedures

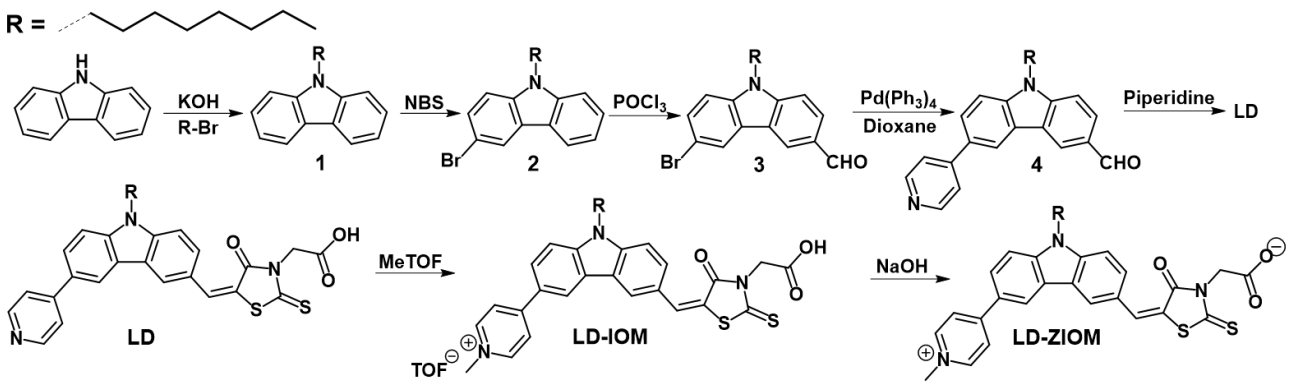

Scheme S1. The synthetic routes of LD, LD-IOM and LD-ZIOM.

Compounds **1-4** and were synthesized according to the reported procedures.[1] Compound **LD** was obtained from aldehyde precursor **4** through Knoevenagel condensation.[2]

(E)-2-(5-((9-octyl-6-(pyridin-4-yl)-9H-carbazol-3-yl)methylene)-4-oxo-2-thioxothiazolidin-3-yl)acetic acid (LD) : Compound 4 (834 mg, 2.44 mmol) and rhodanine-3-acetic acid (695 mg, 3.66 mmol) were added into a solution of ethanol (50 mL) with a catalytic amount of piperidine. Then, the reaction was heated to 90 ℃ and stirred for one night. After cooling down, the mixture was evaporated to dryness. The organic layer was washed with brine for 3 times (100 mL × 3) and extracted with $CHCl_3$ (100 mL × 2), followed by drying over anhydrous $MgSO_4$. The crude product was purified using column chromatography to afford the light yellow-green compound LD (543 mg, yield: 40 %) (Eluent: Hexane / Ethyl acetate =1:2). ^{1}H NMR (400 MHz, DMSO-*d*$_6$) δ 8.87 (s, 1H), 8.61 (d, *J* = 31.8 Hz, 3H), 8.02 (s, 2H), 7.86 (d, *J* = 22.2 Hz, 5H), 4.73 (s, 2H), 4.50 (s, 2H), 1.81 (s, 2H), 1.22 (d, *J* = 36.2 Hz, 10H), 0.80 (s, 3H). MALDI-TOF MS: calcd for $C_{31}H_{31}N_3O_3S_2$, 557.1807; found, 557.3160.

(E)-4-(6-((3-(carboxymethyl)-4-oxo-2-thioxothiazolidin-5-ylidene)methyl)-9-octyl-9H-carbazol-3-yl)-1-methylpyridin-1-ium trifluoromethanesulfonate **(LD-IOM)**: To a 100 mL three-necked round bottom flask was added LD (278 mg, 0.5 mmol) and MeOTF (131 mg, 0.8 mmol) and 10 mL THF. The solution was stirred at room temperature for 2 h and the color of the reaction mixture turned reddish-brown from light yellow. After removing the solvent by rotary evaporateion, crude compound LD-IOM was washed with diethy ether and recrystallized in methanol in sequence. The green-yellow solid (Yield: 162 mg, 45%) was obtained. ^{1}H NMR (400 MHz, DMSO-d$_6$) δ 9.00 (d, J = 21.5 Hz, 2H), 8.65 (s, 1H), 8.58 (s, 1H), 8.31 (s, 2H), 8.17 (s, 2H), 7.88 (s, 3H), 4.53 (s, 2H), 4.32 (s, 2H), 2.85 (s, 3H), 1.81 (s, 2H), 1.23 (dd, J = 21.2, 15.8 Hz, 11H), 0.81 (s, 3H). MALDI-TOF MS: calcd for $[C_{32}H_{34}N_3O_3S_2]^+$, 572.2036; found, 572.5440.

(E)-2-(5-((6-(1-methylpyridin-1-ium-4-yl)-9-octyl-9H-carbazol-3-yl)methylene)-4-oxo-2-thioxothiazolidin-3-yl)acetate **(LD-ZIOM)**: To a 100 mL three-necked round bottom flask were added LD-IOM (216 mg, 0.3 mmol) and 10% sodium hydroxide solution (5 mL). The solution was stirred at room temperature for 2 days. The solid was filtrated and washed with 30 mL cold water. The crude product was recrystallized in methanol and the yellow solid was given (Yield: 137 mg, 80%). ^{1}H NMR (400 MHz, DMSO-d$_6$) δ 9.22 (s, 1H), 8.99 (s, 3H), 8.67 (s, 2H), 8.30 (s, 1H), 7.94 (dd, J = 31.5, 22.7 Hz, 4H), 4.65 (s, 2H), 4.53 (s, 2H), 4.32 (s, 3H), 1.82 (s, 2H), 1.23 (d, J = 40.3 Hz, 10H), 0.81 (s, 3H). MALDI-TOF MS: calcd for $C_{32}H_{33}N_3O_3S_2$, 571.1958; found, 571.5482.

Results and Discussion

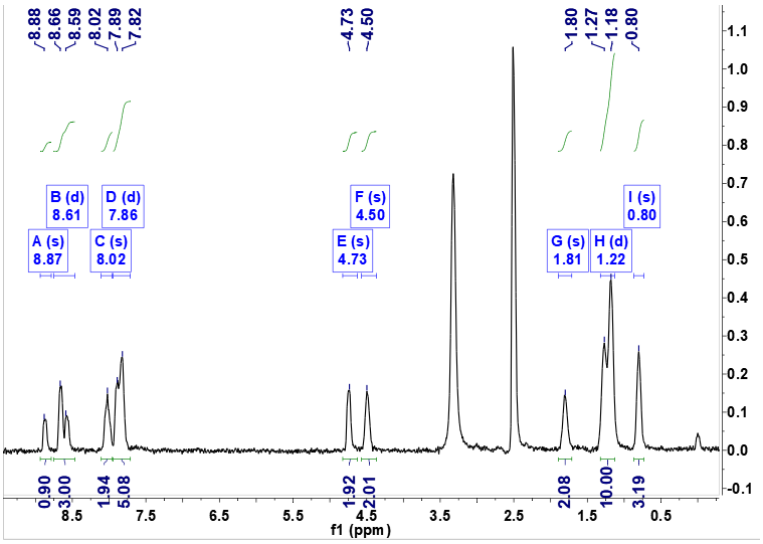

Figure S1. The ^{1}H NMR spectra of LD in DMSO-*d*$_6$.

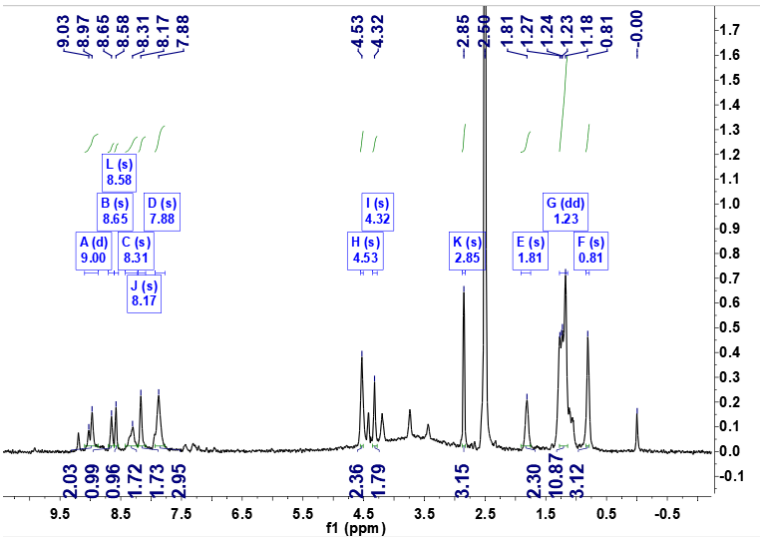

Figure S2. The ^{1}H NMR spectra of LD-IOM in DMSO-d_6.

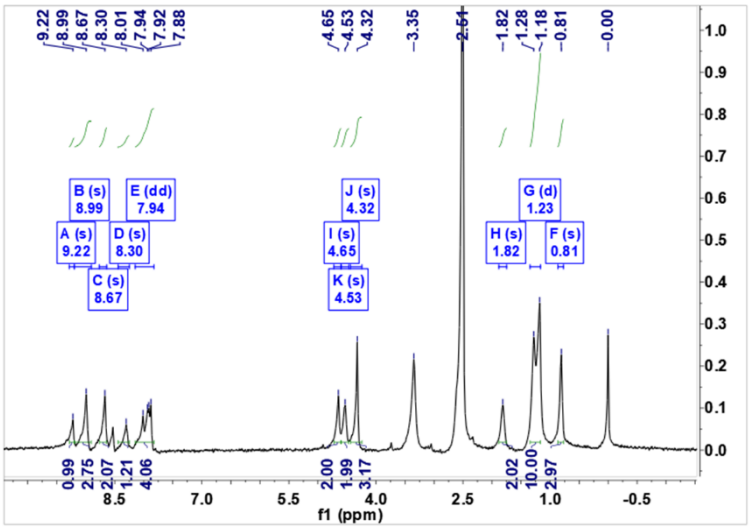

Figure S3. The ^{1}H NMR spectra of LD-ZIOM in DMSO-d_6.

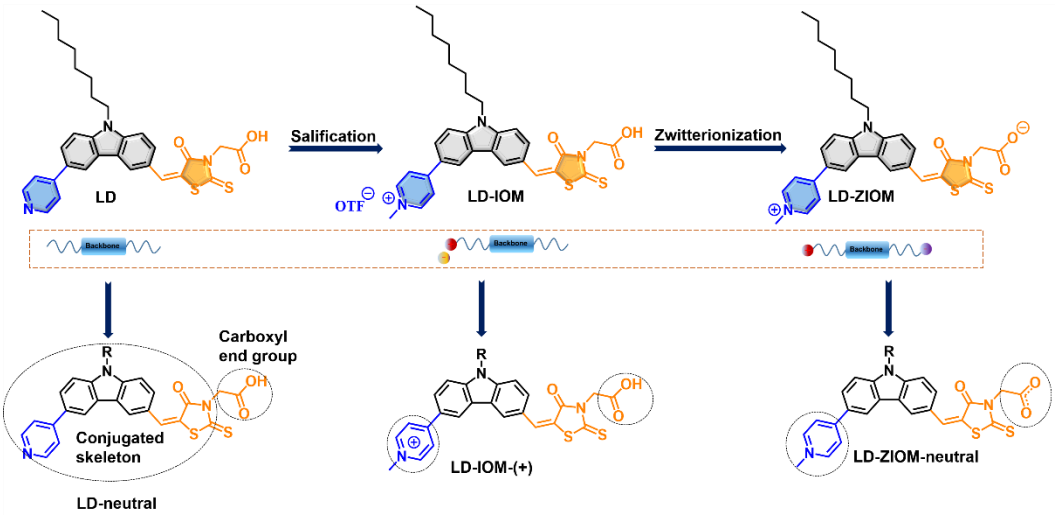

Figure S4. The molecular structures of LD, LD-IOM, and LD-ZIOM (top) and their corresponding prototype structures for theoretical calculations (bottom).

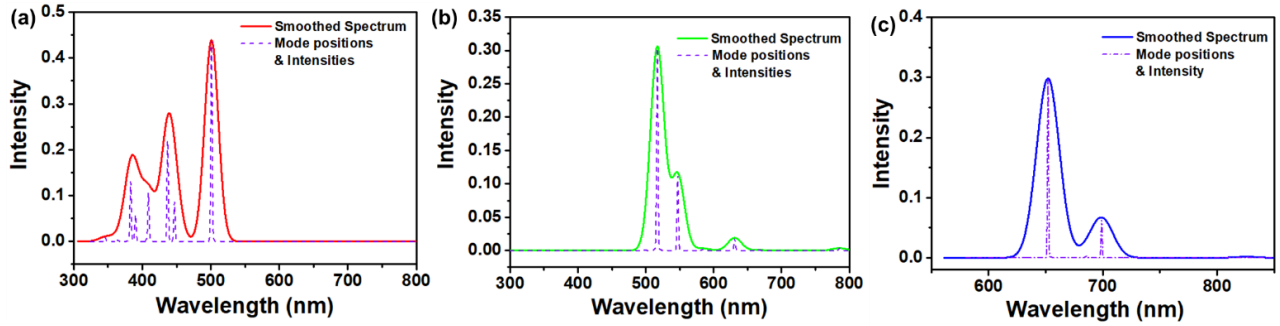

Figure S5. Calculated optical absorption spectra for LD-IOM, LD-ZIOM in DCM solution at GGA/BLYP/DNP (basis file = 4.4) (n states = 12) level of theory: (a) LD. (b) LD-IOM. (c) LD-ZIOM.

Table S1. The detailed descriptions of electronic transitions for LD calculated by TD-DFT method (orbital 147 = HOMO, orbital 148 = LUMO)

From	To	TD-ex[a] (eV)	KS-ex[b] (eV)	TD-ex[c] (eV)	KS-ex[d] (eV)	f_osc[e]	overlap[f]
147	148+	1.85	1.97	670	630	0.068012	0.67
146	148+	2.08	1.97	596	630	0.076455	0.31
146	148-	2.21	2.13	562	582	0.000081	0.31
144	148+	2.41	2.13	514	582	0.000000	0.53
147	148-	2.45	2.46	505	504	0.454384	0.67
145	148+	2.46	2.46	503	504	0.000002	0.23
145	148-	2.47	2.50	503	497	0.006847	0.23
143	148+	2.74	2.50	452	497	0.000000	0.64
144	148-	2.76	2.84	449	437	0.434204	0.53
147	149+	2.97	2.84	417	437	0.000000	0.52
142	148+	3.01	3.03	413	409	0.000004	0.64
143	148-	3.04	3.03	408	409	0.057541	0.64

[a] Time dependent density functional theory (TDDFT) excitation energies. [b] Kohn-Sham (KS) excitation energies. [c] TDDFT excitation wavelength. [d] Kohn-Sham (KS) excitation wavelength. [e] oscillator strengths. [f] The extent of overlap between the electron increasing/decreasing regions.

Table S2. The detailed descriptions of electronic transitions for LD-IOM calculated by TD-DFT method (orbital 151 = HOMO, orbital 152 = LUMO).

From	To	TD-ex [a] (eV)	KS-ex[b] (eV)	TD-ex[c] (eV)	KS-ex[d] (eV)	f_osc[e]	overlap[f]
151	152+	0.68	0.24	1834	5077	0.171840	0.60
151	152+	1.06	1.04	1168	1195	0.013685	0.60
151	152+	1.40	1.39	885	895	0.003711	0.60
151	153+	1.52	1.45	816	855	0.006963	0.68
151	153+	1.72	1.71	720	724	0.000900	0.68
151	152+	1.88	1.81	658	686	0.137831	0.60
151	153+	1.98	2.05	626	604	0.019357	0.68

150	152+	2.16	2.05	575	604	0.000158	0.21
151	153+	2.28	2.16	545	575	0.072545	0.68
149	152+	2.36	2.25	526	551	0.000607	0.64
149	152+	2.37	2.36	524	525	0.213315	0.64
150	153+	2.37	2.37	522	524	0.000096	0.25

[a] Time dependent density functional theory (TDDFT) excitation energies. [b] Kohn-Sham (KS) excitation energies. [c] TDDFT excitation wavelength. [d] Kohn-Sham (KS) excitation wavelength. [e] oscillator strengths. [f] The extent of overlap between the electron increasing/decreasing regions.

Table S3. The detailed descriptions of electronic transitions for LD calculated by TD-DFT method (orbital 151 = HOMO, orbital 152 = LUMO).

From	To	TD-ex [a] (eV)	KS-ex[b] (eV)	TD-ex[c] (eV)	KS-ex[d] (eV)	f_osc[e]	overlap[f]
151	152-	1.50	1.50	827	827	0.000000	0.06
151	152+	1.50	1.50	826	827	0.000587	0.06
150	152-	1.70	1.73	731	719	0.000000	0.38
150	152+	1.77	1.73	699	719	0.021870	0.38
149	152-	1.79	1.80	692	689	0.000000	0.34
151	153+	1.80	1.80	690	689	0.000000	0.12
148	152-	1.81	1.81	687	685	0.000000	0.14
151	153+	1.81	1.81	686	685	0.001069	0.12
148	152+	1.82	1.81	681	685	0.000494	0.14
149	152+	1.90	1.81	652	685	0.099413	0.34
150	153+	1.94	2.03	639	612	0.000000	0.56
149	153-	2.06	2.03	601.	612	0.000000	0.51

[a] Time dependent density functional theory (TDDFT) excitation energies. [b] Kohn-Sham (KS) excitation energies. [c] TDDFT excitation wavelength. [d] Kohn-Sham (KS) excitation wavelength. [e] oscillator strengths. [f] The extent of overlap between the electron increasing/decreasing regions.

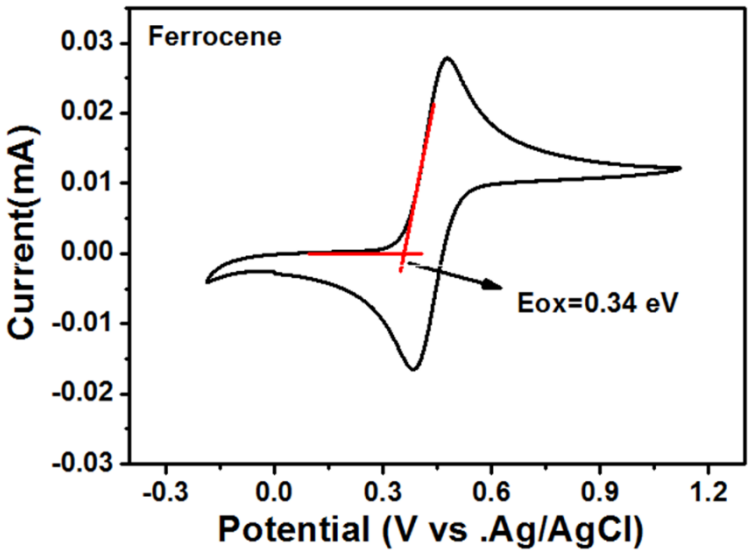

Figure S6. The CV curve of the ferrocene standard at a sweep rate of 100 mV^{-1}.

Table S4. Experimental optical and electrochemical properties of LD, LD-IOM and LD-ZIOM.

Compound	Eg (eV)[a]	HOMO[b] (eV)	LUMO[c] (eV)	ΦITO-HOMO[d] (eV)	LUMO-ΦAl [e] (eV)
LD	2.61	-5.72	-3.11	0.92	1.19
LD-IOM	2.88	-5.52	-3.11	0.92	1.66
LD-ZIOM	3.04	-5.66	-2.62	0.72	1.68

[a] Estimated from the onset of UV−vis absorption by the equation Eg = 1240/λonset. [b] LUMO = HOMO + Eg. [c] HOMO = −(4.80 − $E_{Fc/Fc+}$ + Eox). [d] E_{hole} ΦITO − HOMO. [e] Eelectron = LUMO − ΦAl.

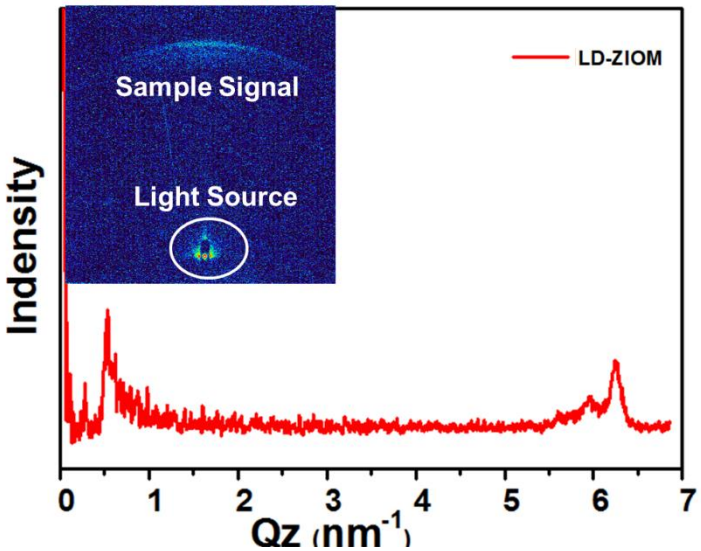

Figure S7. The curve of out-of-plane (Qz) integration that obtained from GISAXS patterns. The inserted image is a GISAXS pattern of LD-ZIOM films cast on ITO film applying an incident beam with a glancing angle of α = 0.20°.

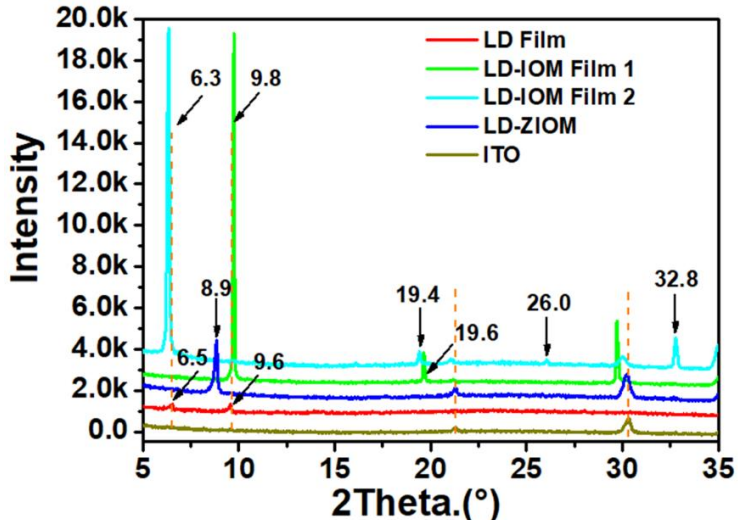

Figure S8. X-ray diffraction patterns of different compounds on ITO basement. LD-IOM film 1 and film 2 were fabricated from hydrophilic acetonitrile and hydrophobic o-dichlorobenzene solvents, respectively.

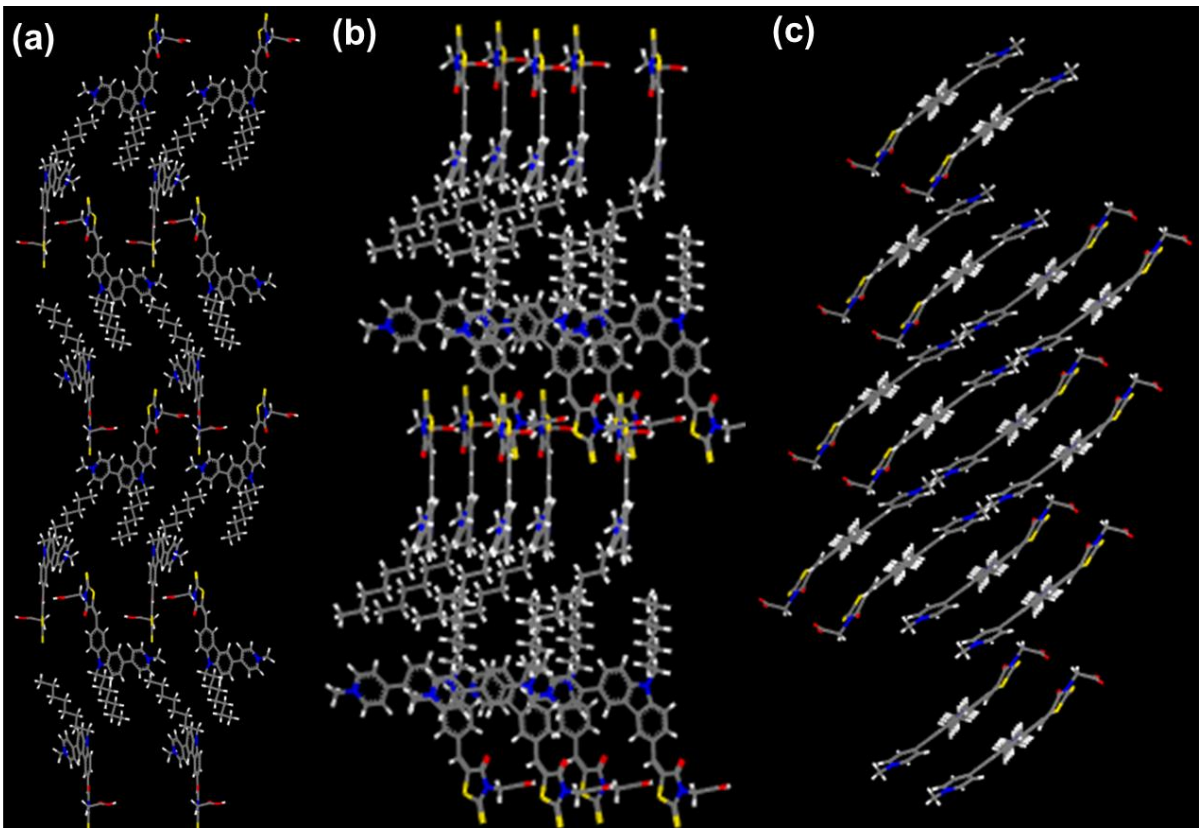

Figure S9. Side view of molecular packing of the molecules revealed by molecular dynamics simulation. (a) LD. (b) LD-IOM. (c) LD-ZIOM.

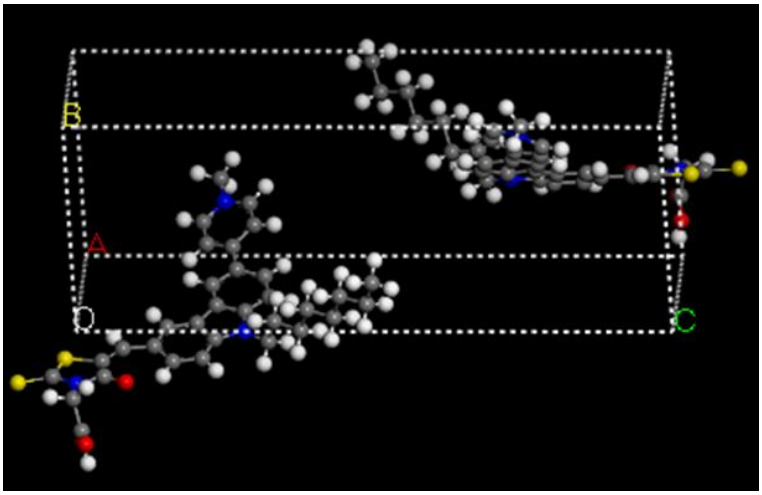

Figure S10. Molecular packing cell unit of LD revealed by molecular dynamics simulation.

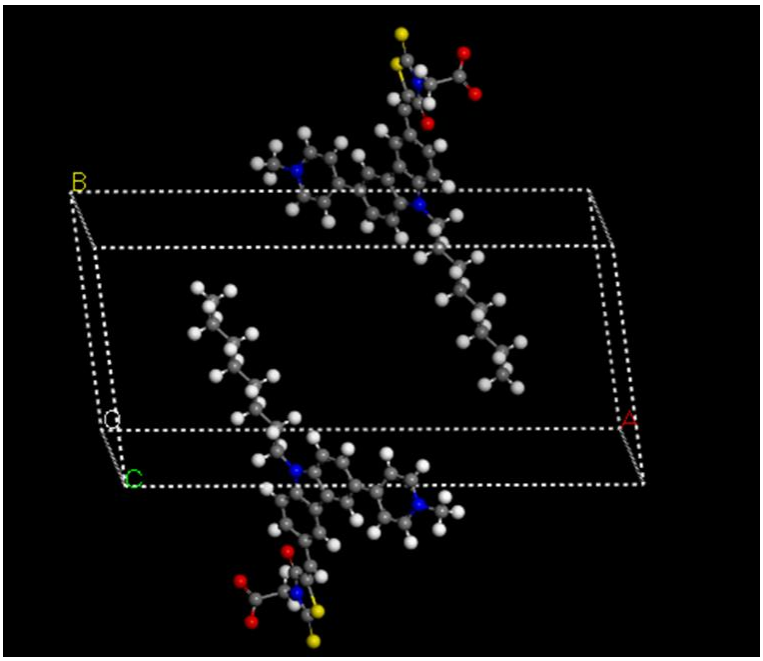

Figure S11. Molecular packing cell unit of LD-IOM revealed by molecular dynamics simulation.

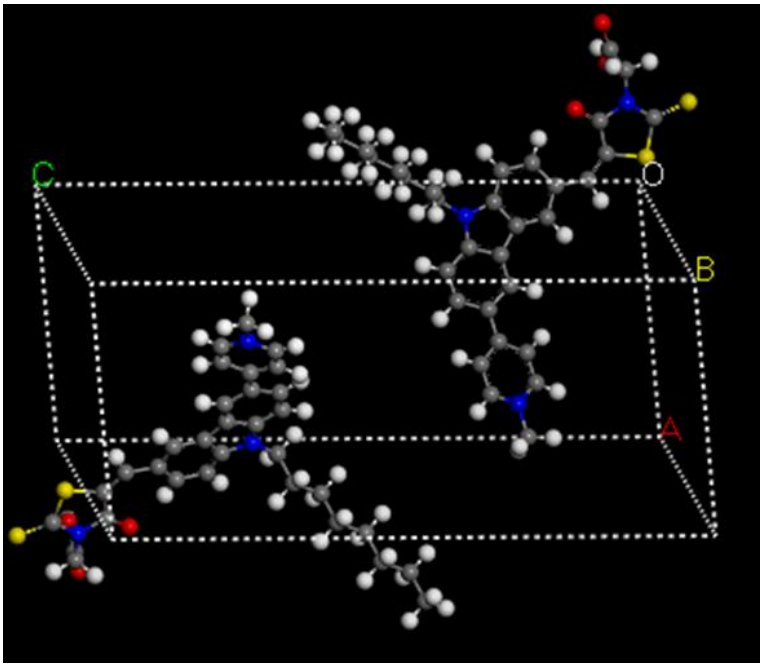

Figure S12. Molecular packing cell unit of LD-IOM revealed by molecular dynamics simulation.

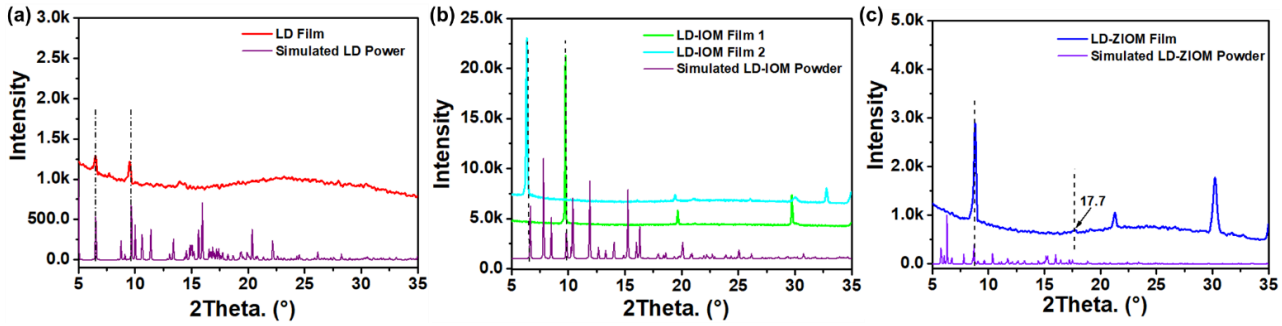

Figure S13. XRD patterns of the materials indexed from the simulated molecular packing: (a) LD. (b) LD-IOM. (c) LD-ZIOM.

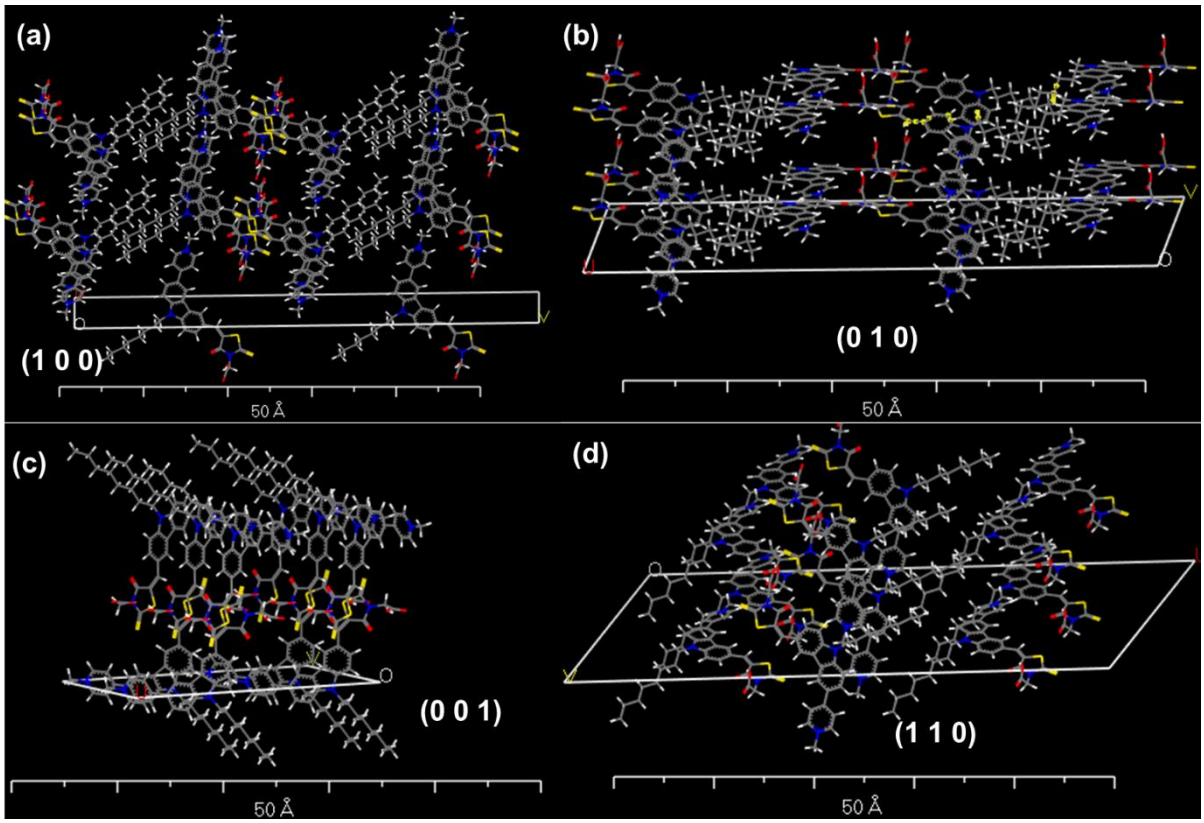

Figure S14. Cleaved lattice plane of LD-IOM from the simulated molecular packing: (a) (1 0 0) reflection. (b) (0 1 0) reflection. (c) (0 0 1) reflection. (d) (1 1 0) reflection.

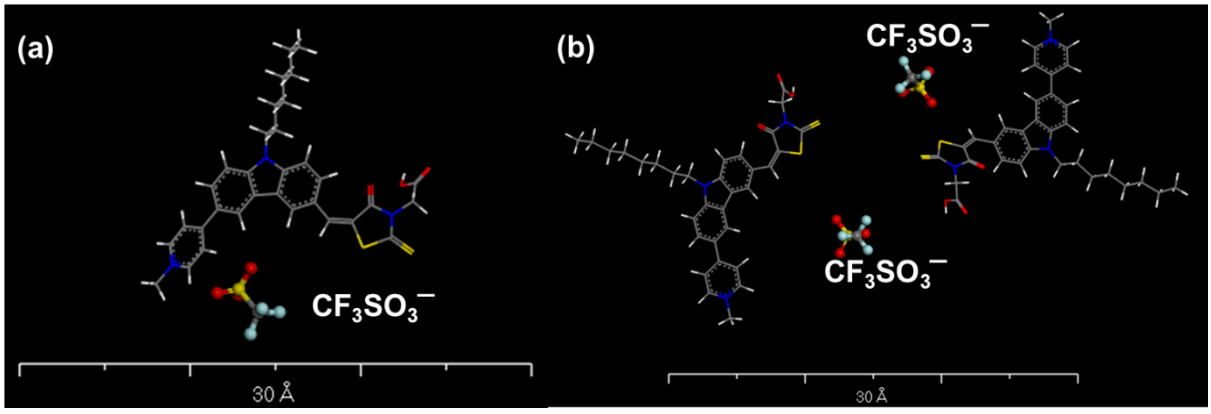

Figure S15. Optimized representative aggregates of LD-IOM and OTF^- calculated in Adsorption Locator module: (a) One LD-IOM and OTF^- cell unit. (b) Two LD-IOM and OTF^- cell unit.

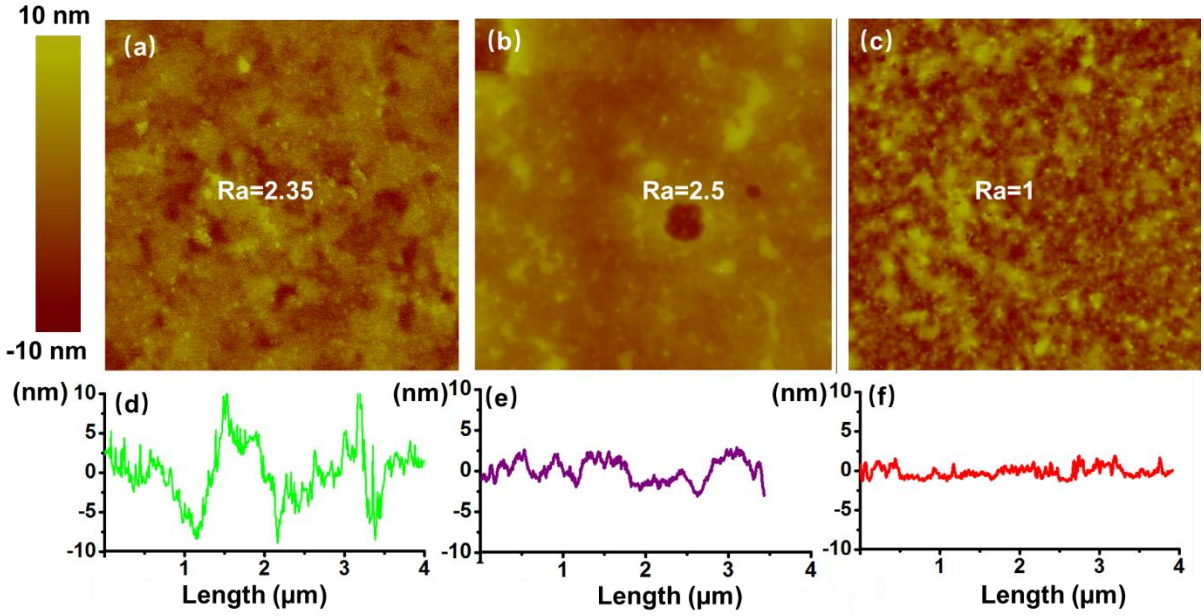

Figure S16. (a-c) Morphology characterization of TM-AFM topographic images and (c-f) of LD, LD-IOM, LD-ZIOM films spin-coated on ITO substrates, respectively. The scan size for both images is 4 μm × 4 μm.

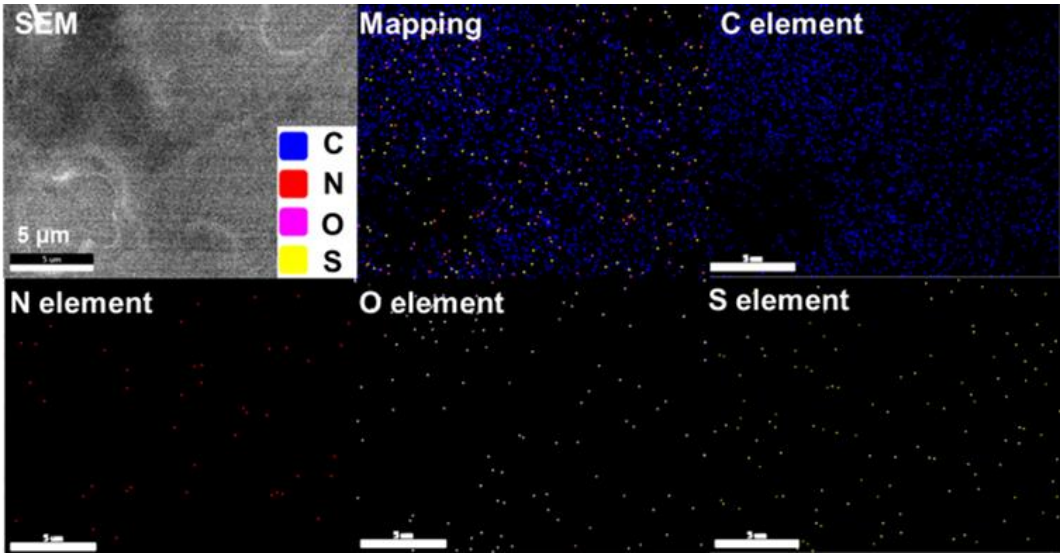

Figure S17. The SEM elemental mapping of the characteristic elements in the LD-based film.

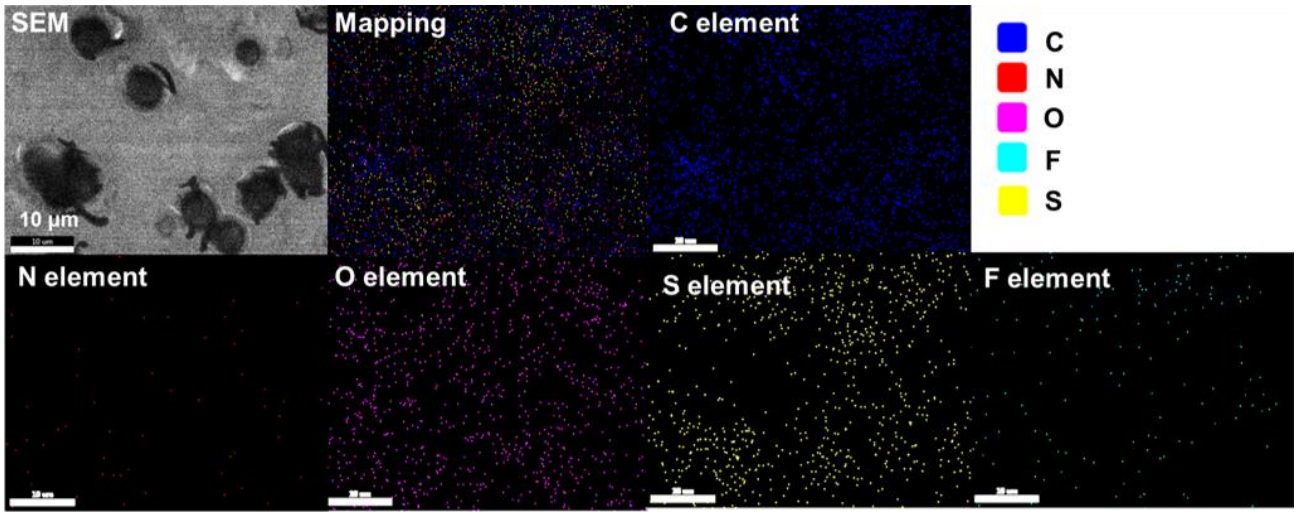

Figure S18. The SEM elemental mapping of the characteristic elements in the LD-IOM-based film.

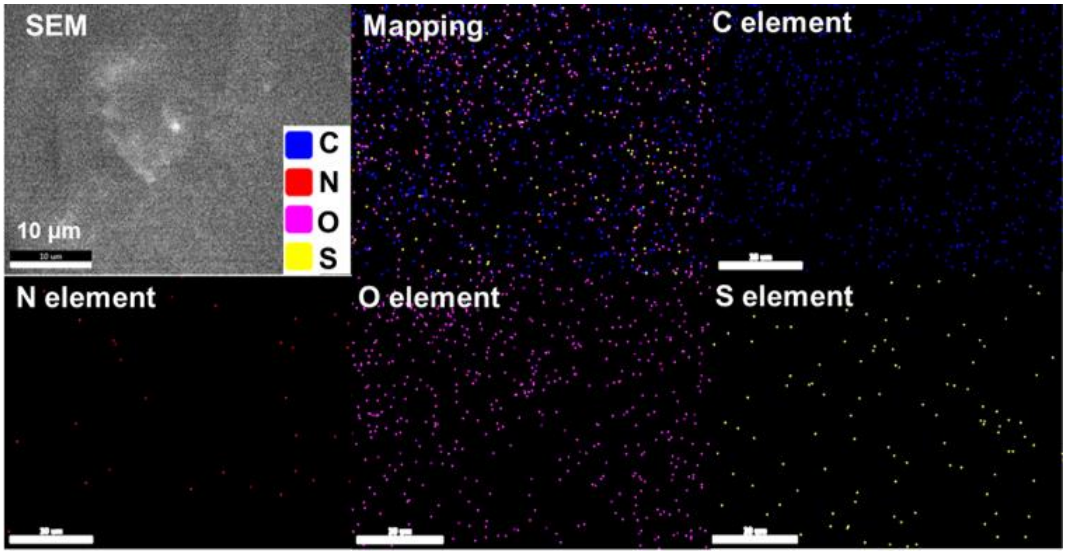

Figure S19. The SEM elemental mapping of the characteristic elements in the LD-ZIOM-based film.

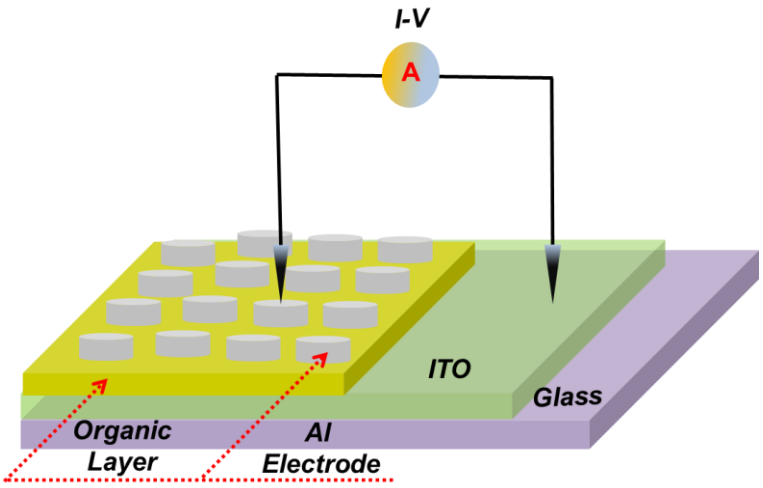

Figure S20. Schematic diagram of the ITO/Organic Layer/Al sandwich structural resistive memory device.

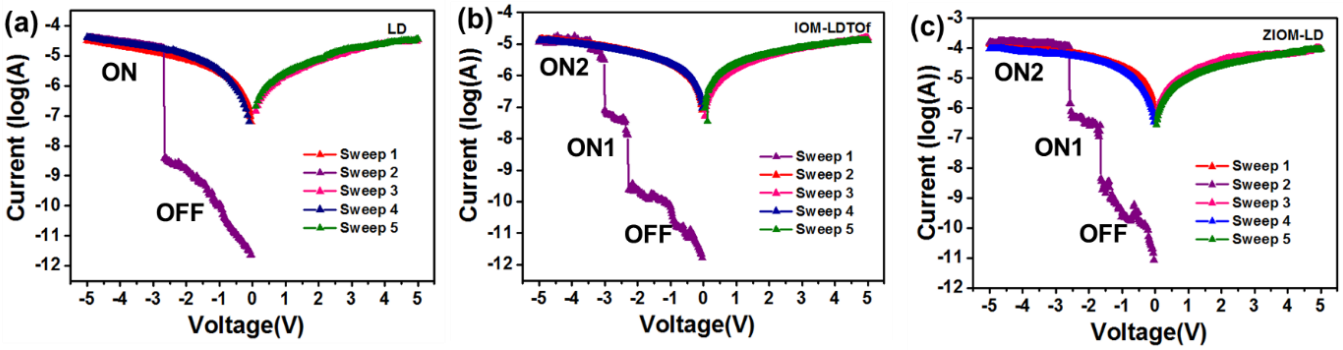

Figure S21. Current-voltage (I-V) characteristics of the sandwich-structured memory devices: (a) LD, (b) LD-IOM, (c) LD-ZIOM.

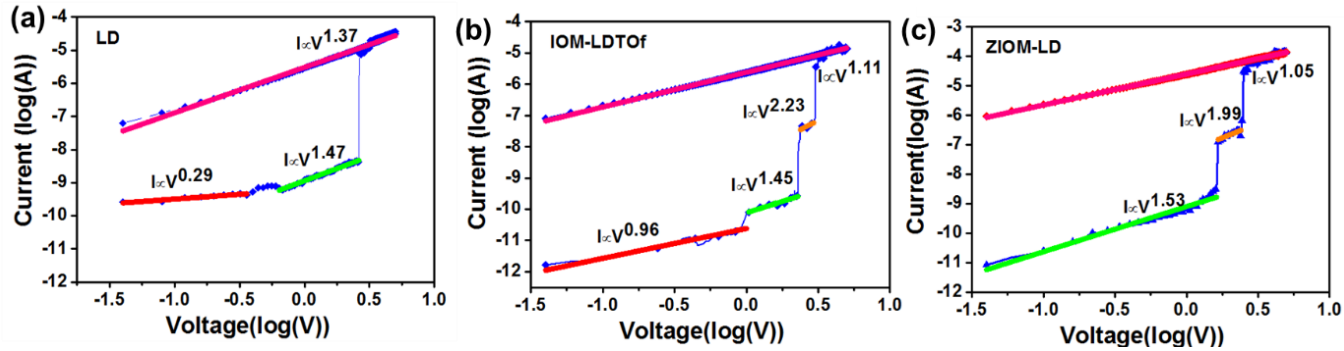

Figure S22. Typical current-voltage relation in log (I)-log (V) plot of as-fabricated memory device： (a) LD, (b) LD-IOM, (c) LD-ZIOM.

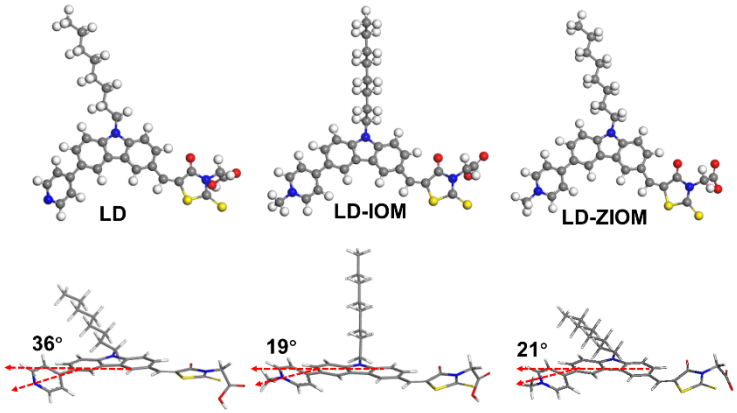

Figure S23. The DFT-calculated dihedral angles of LD, LD-IOM and LD-ZIOM.

Table S5. The DFT-simulated HOMO and LUMO of LD, LD-IOM and LD-ZIOM.

Compound	HOMO (eV)	LUMO (eV)
LD	-4.92	-2.99
LD-IOM-(+)	-6.78	-6.06
LD-ZIOM	-4.12	-3.34

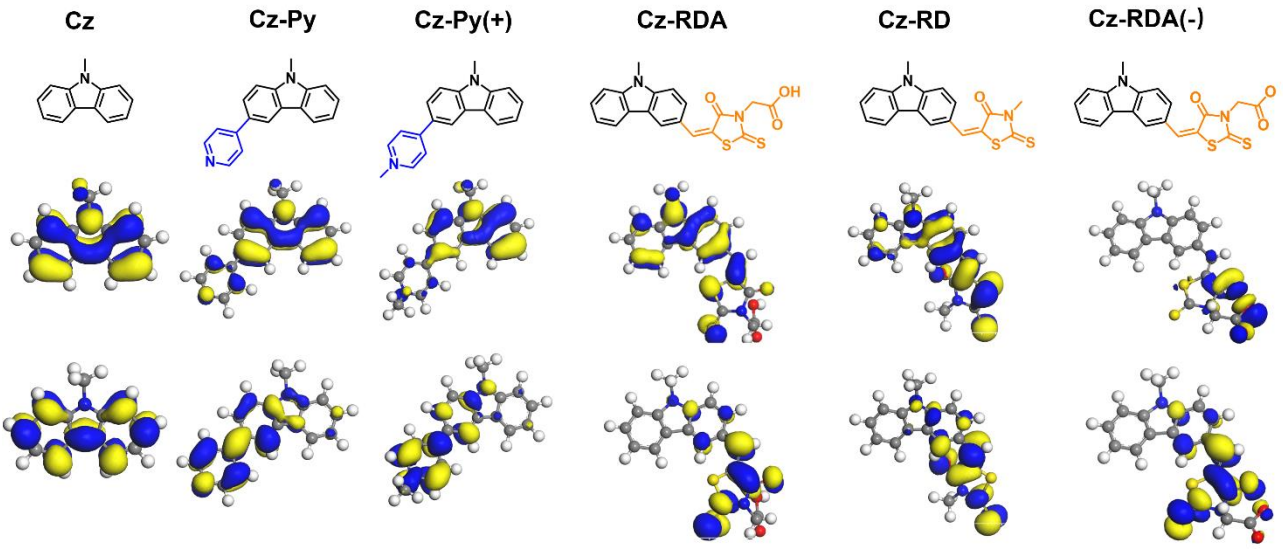

Figure S24. The molecules structures of Cz, Cz-Py, Cz-Py(+), Cz-RD, Cz-RDA and Cz-RDA(-), and their HOMO and LUMO energy levels.

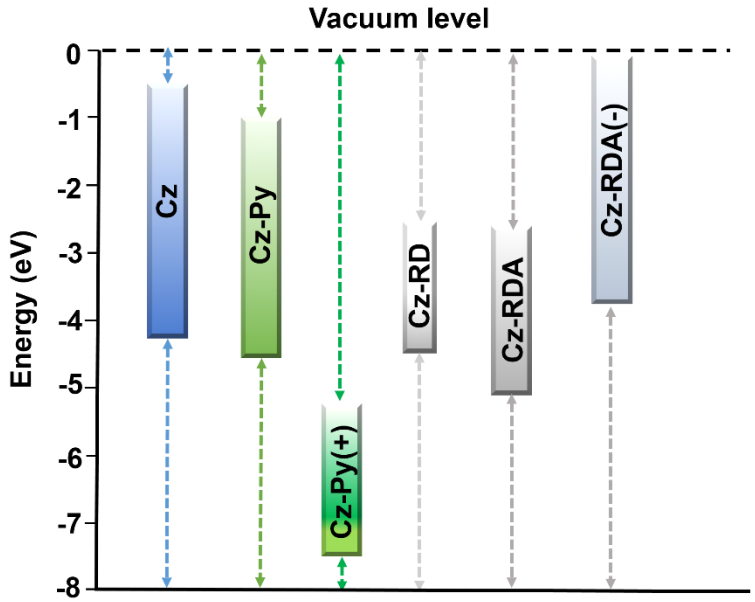

Figure S25. The DFT-calculated electron-withdrawing capability of Cz, Cz-Py, Cz-Py(+), Cz-RD, Cz-RDA and Cz-RDA(-).

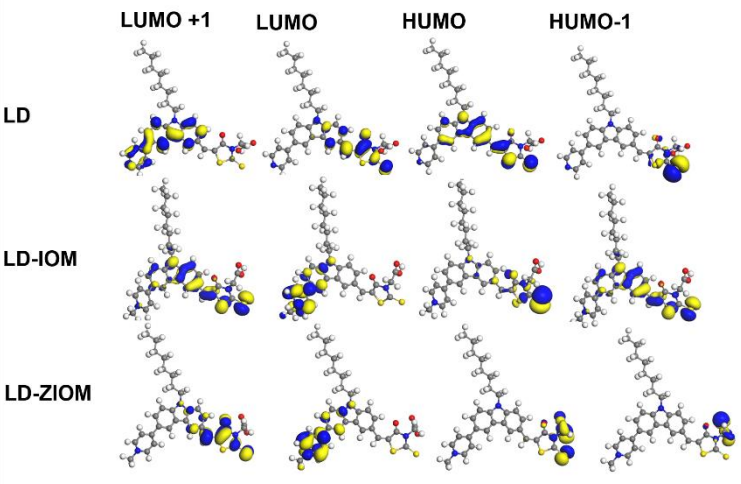

Figure S26. The DFT-calculated HOMO-1, HOMO, LUMO, LUMO+1 of LD, LD-IOM and LD-ZIOM.

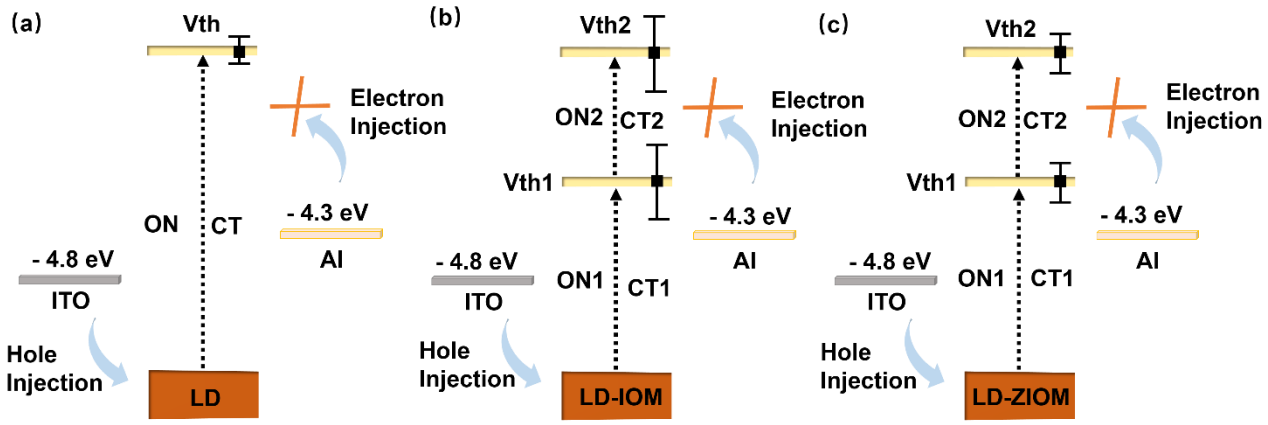

Figure S27. Schematic diagram of the charge injection process in LD, LD-IOM and LD-ZIOM based memory device.

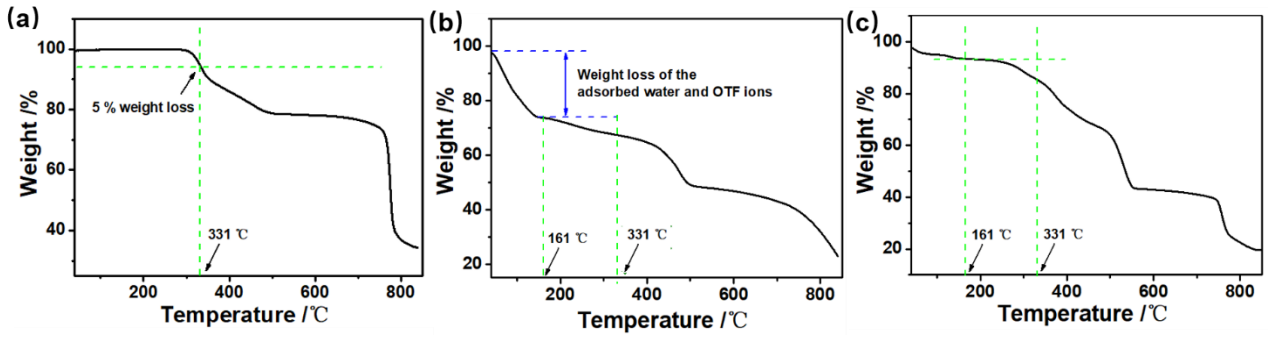

Figure S28. TGA thermograms of (a) LD, (b) LD-IOM, (c) LD-ZIOM. Heating rate: 10 ℃ min−1, under a nitrogen atmosphere.

References

1 a) C. Zhang, H. Li, Y. Su, Q. Zhang, Y. Li and J. Lu, Controllable and versatile electrophoretic deposition technology for monolithic organic memory devices, *ACS Appl. Mater. Interfaces*, 2020, **12**, 15482-15490; b) Z. Liu, J. He, H. Li, Q. Xu, N. Li, D. Chen, L. Wang, X. Chen, K. Zhang and J. Lu, Organic multilevel memory devices of long-term environmental stability via incorporation of fluorine, *Adv. Electron. Mater.,* 2016, **2**, 1500474.

2 S. S. M. Fernandes, M. C. R. Castro, A. I. Pereira, A. Mendes, C. Serpa, J. Pina, L. L. G. Justino, H. D. Burrows, M. M. M. Raposo, Optical and photovoltaic properties of thieno[3,2-b]thiophene-based push-pull organic dyes with different anchoring groups for dye-sensitized solar cells, *ACS Omega,* 2017, **2**, 9268-9279.